

Structural and Optical Features of Sago Starch Polymer Nanocomposites Embedded with Silicon Carbide Nanoparticles

Savita, Navneet Kaur, Jaspreet Kaur, & Annu Sharma*

Department of Physics, Kurukshetra University, Kurukshetra 136 119, India

Received: 10 May 2023; Accepted: 30 May 2023

In the present work, biodegradable polymer sago starch based polymer nanocomposite films reinforced with Silicon Carbide (SiC) nanoparticles were synthesized via solution casting method. The resulting polymer nanocomposite films were characterized utilising transmission electron microscopy, X-ray diffraction, UV-VIS-NIR absorption spectroscopy and dielectric spectroscopy. The data obtained from UV-VIS-NIR absorption spectrophotometer was further used to compute optical parameters such as absorption coefficient (α), optical energy gap (E_g) and Urbach's energy (E_U). Further the transmittance spectra of sago-starch SiC nanocomposite film displayed a sharp decrease in UV region and it decreased from 83.68% to 12.70% at wavelength of 600 nm. E_g of sago-starch film decreased from 4.31 eV to 2.57 eV and E_U increased from 0.66 eV to 1.6 eV with addition of 1 wt% of SiC nanoparticle in sago starch. This is attributed to the additional defects created in HOMO-LUMO gap of polymer matrix. Dielectric spectroscopy results were used to compute dielectric permittivity and dielectric tangent loss. The dielectric permittivity of sago starch increased with addition of SiC nanoparticles while dielectric tangent loss increased at lower frequencies and decreased at higher frequencies and the relaxation peak moved towards the high-frequency side suggesting a decrease in relaxation time.

Keywords: Nano composites, Sago-starch, Optical band gap, Urbach's energy, Dielectric permittivity, Dielectric tangent loss

1 Introduction

In current scenario, the advanced functional materials such as nanocomposites (NCs) are gaining substantial attention of researchers as these materials have superior physical and chemical properties in comparison to the individual components. Due to these interesting properties NCs have broad range of applications such as in photovoltaic, optoelectronics, energy storage, super capacitors, flame retardants, sensors etc¹. With an increasing global awareness about non- biodegradable materials such as plastics, there is a need for environment friendly materials such as biodegradable polymers. Thus, replacement of the non-degradable plastics with biodegradable polymers is an efficient strategy for the management of waste and maintaining environmental health². Biodegradable polymer nanocomposites (PNCs) comprises of fillers (inorganic) as nanoparticles (NPs) and biodegradable polymer as host matrix (organic) results in improving some of the inherent shortcomings of polymers such as low mechanical strength and electrical conductivity³. The natural biopolymers such as gelatin, sodium alginate, starch, cellulose, chitosan etc. have low cost, highly

abundant, biodegradable, renewable, environment friendly and non-toxic in nature, hence, efforts have been made to combine organic polymeric materials with inorganic materials, to fabricate tailored materials with desired attributes⁴. Among various biopolymers, starch, a natural-derived polysaccharide is abundantly available as it can be easily extracted from roots, stems, and seeds of rice, wheat, cassavas, corns, potatoes, etc. Its molecular structure consists of amylose and amylopectin having glycosidic bond linkages⁵. Among the starch materials, sago starch (SG-ST) is obtained from the sago palm tree and has very low cost, excellent film forming ability, bio compatibility as compared to other starch materials^{6,7}. Due to these characteristics, SG-ST films are being explored for application in flexible electronics such as flexible conductive electrodes, transistors, super capacitors, sensors, nanogenerators, etc⁸. Various inorganic nano fillers have been used to enhance the physicochemical, mechanical and thermal properties of the polymers⁹⁻¹³. Among these inorganic nanofillers, SiC is an important wide band-gap (2.4 to 3.3 eV) non-oxide ceramic semiconductor having more than 250 polytypes. Moreover, it has excellent physical and chemical attributes such as high melting point, high chemical stability, smaller thermal expansion

*Corresponding author (E-mail: asharma@kuk.ac.in)

coefficient, high thermal conductivity, better abrasion resistance, superior mechanical properties etc. The SiC NPs have advanced applications in the area of high-temperature sensors, microwave devices and high-power devices¹⁴⁻¹⁶. In earlier studies, Tkaczyk¹⁷ fabricated SiC nanocrystals-Polibutadien NC and observed a rapid increase in the current of the NC when 5 wt % SiC nanocrystals added in to the Polibutadien. Dash *et al.*¹⁸ fabricated Starch-SiC NCs and observed a remarkable reduction in oxygen permeability of the resultant NCs. Saini *et al.*¹⁹ investigated the influence of grafted SiC nanocrystal on the optical, electrical and mechanical properties of polyvinyl alcohol (PVA). Wang *et al.*²⁰ investigated the effect SiC nanofiller on tribological behaviour of polyetheretherketone (PEEK)²⁰. Kisku *et al.*²¹ reported the effect of SiC NPs on cellulose for investigating the oxygen barrier properties and have shown that oxygen permeability was reduced by three times with addition of 10 wt% of SiC in cellulose. This decrease in oxygen permeability might be the manifestation of SiC NPs in the voids of cellulose which restrict the path for oxygen penetration. Pradhan *et al.*²² reported that SiC/Chitosan NCs have potential packaging applications because of their enhanced tensile strength, thermal stability and less oxygen permeability.

Although some reports are available on SiC based biopolymer nanocomposites. However optical and dielectric attributes of SG-ST/SiC NCs have seldom been studied. Thus in the present work an attempts has been made to investigate the impact of SiC on structural, optical and dielectrics attributes of SG-ST.

2 Materials and Methods

2.1 Materials

Nitric acid, glycerol, and ethylene glycol used in the present study for the fabrication of NC films were purchased from Rankem, India. Sago starch was purchased from local market. SiC NPs of size 50-150 nm were fabricated using the solid phase reaction in which carbon was reacted with molten silicon²³.

2.2 Synthesis of Nanocomposite Films

The solution casting technique was employed to synthesize biopolymer based NCs. An appropriate quantity of SG-ST powder was dissolved in deionized water in a round bottom flask (R.B) with glycerol used as a plasticizer. Different wt % of SiC NPs were dissolved in deionized water at 65 °C under constant ultrasonication until homogenous solution obtained.

SG-ST and SiC solution were mixed together under constant stirring using magnetic stirrer at 1000-1500 rpm. The prepared solution was poured in petri dishes and then dried until the solvent evaporated. The resulting NC films were peeled off for further characterization. Pristine SG-ST film was also synthesized in same manner.

2.3 Characterization of Sago-Starch/SiC NC Films

Transmission Electron Microscope (TEM) by "Talos" (operating voltage=200 kV) was used for revealing the size distribution of SiC NPs. X-ray diffraction measurements of the SiC powder sample and SG-ST/SiC NC films were carried out using "Bruker AXS D8 Advance Diffractometer" in the wide region of 10° to 80° at 40 kV and 20 mA. Absorption spectra of pristine SG-ST and SG-ST/SiC NC films were recorded using UV-VIS-NIR Spectrophotometer "Shimadzu Double Beam Monochromator Spectrometer, UV-250" in the range 200 nm to 2000 nm. The obtained data was further analysed to compute optical parameters. The dielectric spectroscopy Instrument "Wayne Kerr 6500B Precision Impedance Analyser" operated in the frequency region of 20 Hz – 1M Hz was used to compute the dielectric parameters of synthesized NC films.

3 Results and Discussion

3.1 TEM Analysis

Figure 1 (a) presents the TEM micrograph of SiC NPs and particle size distribution of SiC NPs is depicted in Fig. 1 (b). According to this micrograph, crystallite size of SiC NPs was obtained using these micrographs is 40.63 ± 2.6 nm¹².

a. XRD Analysis

Figure 2(a) depicts the XRD pattern of SiC NPs. XRD pattern of SiC NPs shows major diffraction peak at 2θ values of 35.36° corresponding (111) plane and other minors peaks at 2θ values of 41.12°, 59.72°, 71.52° and 75.21° which corresponds to (200), (220), (311) and (222) planes respectively of SiC NPs. These characteristic peaks of SiC agree with JCPDS card no. 29-1129²⁴.

Figure 2(b) represents the XRD pattern of pristine SG-ST and SG-ST/SiC NCs films with 1 and 5 wt% of SiC NPs represented by SS0, SS1 and SS5 respectively. XRD pattern of pristine SG-ST(SS0) shows diffraction peaks at 2θ values of 16.84°, 19.54°, 21.81° which are the characteristic peaks of SG-ST. XRD pattern of SG-ST/SiC NC films, displays the

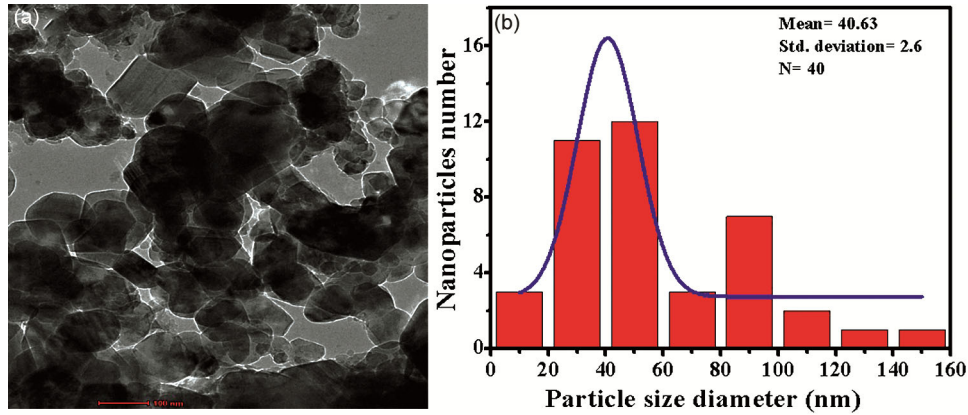


Fig. 1 — (a) TEM micrograph of SiC NPs, and (b) particle size distribution of SiC NPs.

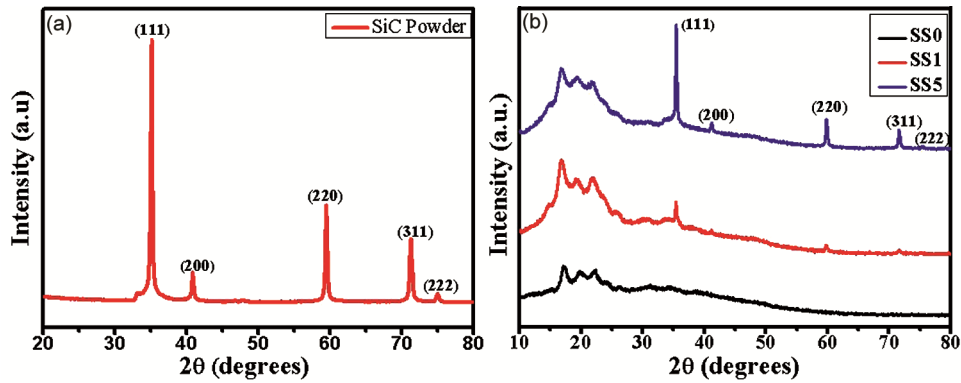


Fig. 2 — (a) XRD pattern of SiC NPs, and (b) SS0, SS1 and SS5 NC films.

characteristic peaks of SG-ST at 2θ values of 16.91° , 19.35° and 21.81° and of SiC at 2θ value of 35.48° corresponding to (111) plane and other minors peaks of SiC at 2θ values of 41.33° , 59.83° , 71.64° and 75.35° which corresponds to (200), (220), (311) and (222) planes respectively.

W-H method²⁵ was used to compute the lattice strain along with crystallite size using equation 1:

$$\beta_t \cos\theta = \frac{0.9\lambda}{t} + 4\epsilon \sin\theta \quad \dots(1)$$

where ‘ λ ’ is the wavelength of Cu K_α radiation, ‘ t ’ is the crystallite size of NPs and ‘ β_t ’ is the full width of half maxima of diffraction peaks. A graph between $4\sin\theta$ along x-axis and $\beta_t \cos\theta$ along Y-axis has been plotted for SS5 NC film as shown in Fig. 3. Lattice strain and crystallite size has been calculated from slope and intercept of best fit line data.

The average crystallite size of SiC NPs in SS5 NC film comes out to be 37.48 nm and is agreement with TEM measurements. The positive value of slope indicates the expansion of lattice and intrinsic lattice strain comes out to be 2.8×10^{-3} .

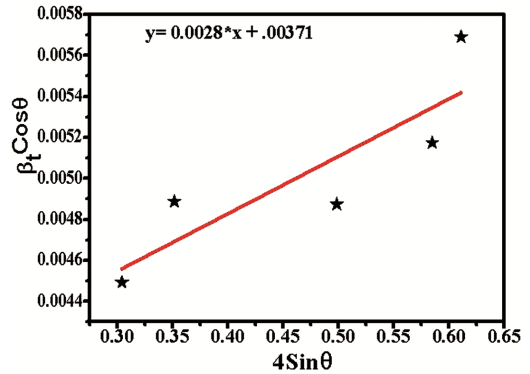


Fig. 3 — Plot of $\beta_t \cos\theta$ versus $4 \sin\theta$ for SS5 NC film.

3.3 Optical Parameter Measurements

Figure 4 represents the absorption and transmittance spectra of SS0, SS1 and SS5 NC films. It clearly depicts that absorption of SG-ST film increases while transmittance decreases with the addition of SiC NPs. Further absorption edge is well defined in Fig. 4(a) thus confirming the semi-crystalline nature of SG-ST. This absorption edge is shifted towards higher wavelength on the addition of SiC NPs in SG-ST. Figure 4(b) represents the transmittance spectra of SS0, SS1 and SS5 NC film

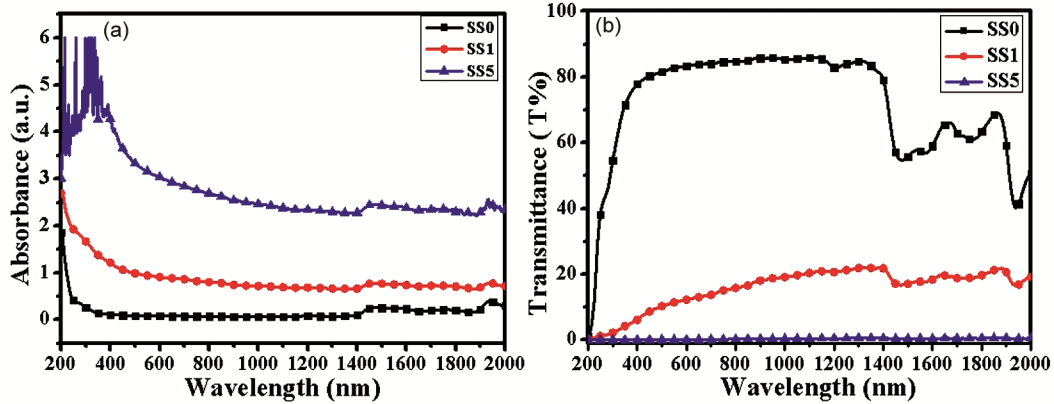


Fig. 4 — (a) Absorbance, and (b) transmittance spectra of SS0, SS1 and SS5NC films.

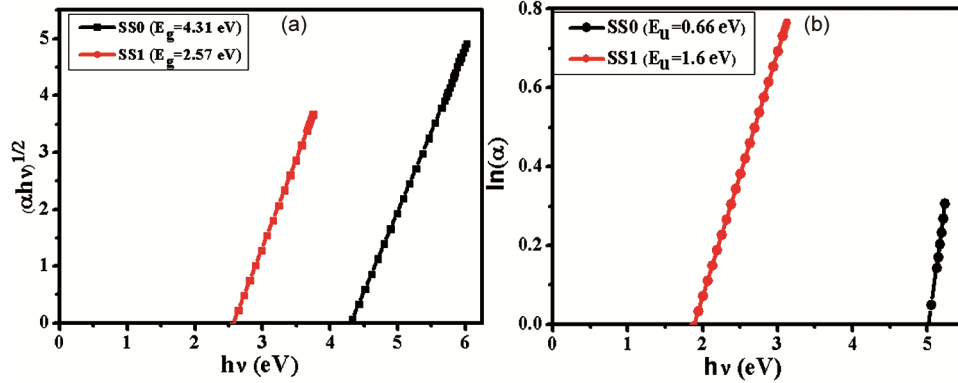


Fig. 5 — (a) Plot of $(\alpha hv)^{1/2}$ versus $h\nu$, and (b) plot of $\ln(\alpha)$ versus $h\nu$ for SS0 and SS1 NC films.

and it demonstrates a appreciable decrease in transmittance in UV region and it decreases from 83.68% (SS0) to 12.70% (SS1) at a wavelength of 600 nm^{26,27}.

3.3.1 Optical Band Gap and Urbach’s Energy

The UV-VIS-NIR absorption data was further analysed to compute absorption coefficient ‘ α ’. The Beer Lambert’s law relates α with absorbance ‘ A ’ and thickness ‘ t ’ of the film by equation 2:

$$\alpha = 2.303 \frac{A}{t} \quad \dots(2)$$

The value of ‘ α ’ was further used to calculate the HOMO-LUMO (Highest occupied Molecular Orbital-Lowest Unoccupied Molecular Orbital) gap also known as optical energy gap(E_g) using Taucrelation given by equation 3²⁸:

$$\alpha hv = B(hv - E_g)^n \quad \dots(3)$$

where ‘ B ’ is constant, ‘ $h\nu$ ’ is the photon energy and the value of ‘ n ’ decided by the nature of the transition. When $n=1/2, 3/2, 2$ or 3 the nature of the transition is allowed direct, forbidden direct, allowed indirect or forbidden indirect transition. A graph was

Sr. No.	NC Film	E_g (eV)	E_U (eV)
1.	SS0	4.31	0.66
2.	SS1	2.57	1.6

plotted among $(\alpha hv)^{1/2}$ and $h\nu$, when the best fit line is extrapolated it intersects the ‘ $h\nu$ ’ axis, such that $\alpha=0$ (shown in Fig. 5(a)), and gives the value of E_g . The value of E_g of pristine SG-ST decreased from 4.31eV to 2.57 eV with the addition of 1 wt% of SiC NPs in SG-ST matrix.

Urbach’s energy (E_U) which is a measurement of the disorder produced in the forbidden band gap of the polymer, due to the addition of SiC NPs can be evaluated using Urbach’s formula given in equation 4:

$$\alpha = \alpha_0 \exp \frac{h\nu}{E_U} \quad \dots(4)$$

Where ‘ α ’ represents the absorption coefficient, ‘ α_0 ’ is the constant, ‘ $h\nu$ ’ is the photon energy.

E_u was determined by taking the reciprocal of the slope of best fit line between $\ln(\alpha)$ and $h\nu$ as shown in Fig. 5 (b) and values are listed in Table 1. It was observed that E_U of pristine SG-ST increased from 0.66 eV to 1.6 eV (SS1) after the addition of SiC NPs,

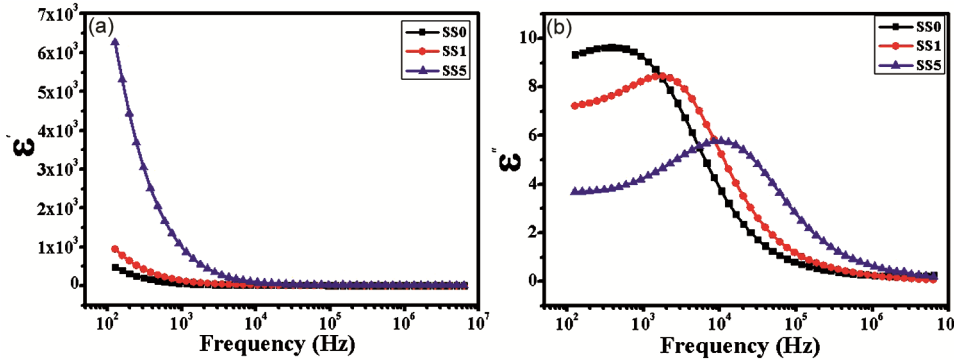


Fig. 6 — Variation of (a) ϵ' , and (b) ϵ'' with frequency for SS0 SS1and SS5 NC films.

which might be due to the generation of defectsites in the forbidden gap of SG-ST.

3.4 Dielectric Parameters

Dielectric spectroscopy reveals the response of a material to static or alternating electric field and measures the dielectric parameter such as permittivity, loss tangent and electric modulus of specimen as a function of the frequency.

The real (ϵ') part of dielectric function known as permittivity, is the measurement of the ability of a material to be polarised in the presence of alternating electric field and the imaginary part of dielectric function (ϵ''), identified as the dielectric loss, is a direct measure of dissipation of energy. Dielectric spectroscopy instrument provides the data of capacitance (C) and dielectric loss which were further utilized to evaluate the permittivity and dielectric loss tangent using equation 5 and 6. In the present study, value of capacitance (C) and ϵ'' were recorded in the frequency region of 20Hz to 1 MHz.

$$\epsilon' = \frac{cd}{\epsilon_0 A} \dots(5)$$

$$\tan\delta = \frac{\epsilon''}{\epsilon'} \dots(6)$$

where ‘d’ and ‘A’ represent thickness and cross-sectional area of the specimen and ‘ ϵ_0 ’ denotes permittivity of free space ($8.854 \times 10^{-12} \text{ Fm}^{-1}$).

Figure 6 represents the behaviours of permittivity (ϵ') and dielectric loss (ϵ'') with frequency for SS0, SS1 and SS5 NC films. It clearly depicts that ϵ' and ϵ'' of pristine SG-ST increases with addition of SiC NPs. The higher value ϵ' at lower frequencies is due to the presence of space charge polarization along with other polarization mechanisms such as orientational, ionic and optical polarization. As the frequency increases first the contribution of space charge polarization diminishes. With further increase in frequency to microwave and subsequently infrared

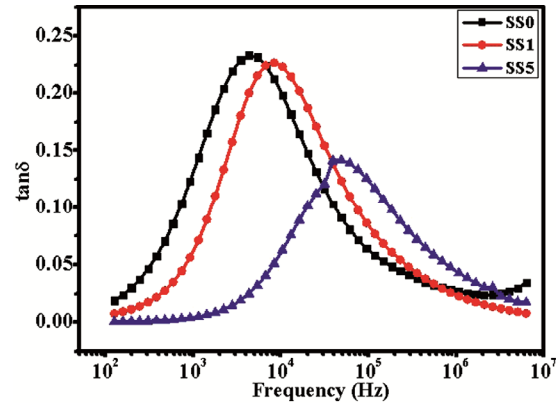


Fig. 7 — Variation of $\tan\delta$ with frequency for SS0, SS1and SS5 NC films.

region contribution of orientational and ionic polarization fades out. At higher frequencies only electronic polarization contributes, as a result, ϵ' attains a constant value as depicted in Fig. 6(a). Figure 6 (b) displays the variation of dielectric loss (ϵ'') with frequency for SS0, SS1and SS5 NC films. It clearly depicts that the value of ϵ'' decreases with increase in concentration of SiC NPs in SG-ST and reaches a maxima in mid-frequency region and then, a decline in the curve is observed with increase in frequency. The dielectric loss is related to the amount of energy required to align the dipoles in the direction of field.

Figure 7 represent the variation of $\tan \delta$ with frequency for SS0, SS1 and SS5. It depicts that, initially, $\tan \delta$ increases, attains a maximum value and finally it decreases with further increase in frequency SG-ST (SS0). Similar behaviour is observed for SS1 and SS5 NC films. In the low frequency region, it is possible for the dipoles to align with the applied field, as a result polarization increases thus $\tan \delta$ also increases. In the mid frequency region, the rotation of dipoles and frequency of the applied electric field matches, a resonance condition is established and

thus, a resonance peak is obtained. At higher frequencies, dipoles are unable to follow the applied field, which results in the decreased values of $\tan \delta$. At resonance, most of the field energy is dissipated in the form of heat. Further, it was observed that the relaxation peak moves towards higher frequencies (as depicted in Fig. 7) with increase in concentration of SiC in pristine SG-ST which indicates that the relaxation time decreases^{29,30}.

4 Conclusion

SG-ST/SiC NC films were successfully synthesized by solution casting technique. According to XRD data analysis, the average crystallite size of SiC NPs comes out to be 37.38 nm which is in good agreement with size obtained via TEM measurement. Optical energy gap of SG-ST decreased from 4.31 to 2.57 eV and Urbach's energy increased from 0.66 to 1.6 eV on incorporation of 1 wt% SiC NPs in SG-ST matrix. The value of dielectric permittivity is higher at lower frequencies due to the presence of space charge polarization mechanism along with the orientational, ionic and electronic polarization. At higher frequencies, dipoles are unable to follow the alternating applied field and orientational and ionic polarization contribution faded out, only electronic polarization contributed, as a result permittivity has a constant value. Dielectric loss decreases with increase in concentration of SiC NPs in SG-ST. Further it observed that the value of tangent loss increased at lower frequencies and decreased at higher frequencies. In the mid frequencies, $\tan \delta$ got a maximum value, thus resonance peak obtained. The relaxation peak shifted toward the higher frequencies with the addition SiC NPs in pristine SG-ST suggesting a decrease in relaxation time.

5 Acknowledgement

Authors would like to take the privilege to thank Department of Science and Technology (DST), New Delhi for providing financial support for installation of X-ray Diffractometer and UV-Visible Spectrometer at Ion Beam Centre, Kurukshetra University, Kurukshetra. Authors are thankful to SAIF- AIIMS for TEM studies. One of the authors (Savita) is thankful to UGC for providing the NET-SRF fellowship for supporting the research work.

References

- 1 B Sharma, P Malik & P Jain, *Mater Today Commun* 16(2018) 353.
- 2 E Matei, A M Predescu, M Răpă, A A Țurcanu, I Mateș, N Constantin & C Predescu, *Nanomaterials*, 12(10)(2022) 1707.
- 3 T Glaskova-Kuzmina, O Starkova, S Gaidukovs, O Platnieks, & G Gaidukova, *Polymers*, 13(19)(2021) 3375.
- 4 R Xiong, A M Grant, R Ma, S Zhang, & V V Tsukruk, *Mater Sci Eng R Rep*, 125(2018)1.
- 5 M P Guarás, L N Ludueña, & V A Alvarez, *Handbook of Nanomaterials and Nanocomposites for Energy and Environmental Applications*, (2020)1.
- 6 M N Abdorreza, L H Cheng, & A A Karim, *Food Hydrocoll*, 25(1) (2011)56.
- 7 F B Ahmad, P A Williams, J L Doublier, S Durand, & A Buleon, *Carbohydr Polym*, 38(4)(1999) 361.
- 8 H Xiang, Z Li, H Liu, T Chen, H Zhou & W Huang, *npj Flex*, 6(1)(2022)1.
- 9 Meena, & A Sharma, *Int J Polym Anal Charact* 26(5)(2021) 396.
- 10 T Soliman, & S A Vshivkov, *Journal of Non-Crystalline Solids*,(2019) 519.
- 11 N S Alghunaim, *Results Phys*,9(2018), 1136.
- 12 I Saini, A Sharma, J Rozra, R Dhiman, S Aggarwal & P K Sharma, *JAppl Polym Sci*, 132(34)(2015).
- 13 J Rozra, I Saini, A Sharma, S Aggarwal, R Dhiman & P K Sharma, *Mater Chem Phys*,134(2-3)(2012) 1121.
- 14 Y Wang, S Dong, X Li, C Hong, & X Zhang, *Ceram Int* (2021).
- 15 H Abderrazak & E S B H Hmida, IntechOpen, (2011).
- 16 Y Li, C Chen, JT Li Y Yang & ZM Lin, *Nanoscale Res Lett* 6 (2011) 454.
- 17 S W Tkaczyk, *Physica E Low Dimens Syst Nanostruct* 43(6) (2011)1179.
- 18 S Dash & S K Swain, *Carbohydr Polym*97(2)(2013) 758.
- 19 I Saini, A Sharma, R Dhiman, S Aggarwal, S Ram & P K Sharma, *J Alloys Compd*, 714(2017), 172.
- 20 Q H Wang, Q J Xue, W M Liu, & J M Chen, *JAppl Polym Sci*, 78(3)(2000) 609.
- 21 S K Kisku, S Dash & S K Swain, *Carbohydr Polym*, 99 (2014), 306.
- 22 G C Pradhan, S Dash & S K Swain, *Carbohydr Polym*, 134(2015) 60.
- 23 R Dhiman, E Johnson, E M Skou, P Morgen & S M Andersen, *J Mater Chem*, 1(19)(2013) 6030.
- 24 Y Wang, Z Iqbal & S Mitra, *Carbon*, 44(13)(2006) 2804.
- 25 D Nath, F Singh & R Das, *Mater Chem Phys*, 239 (2020)122021.
- 26 CSSR Kumar, *UV-VIS and Photoluminescence Spectroscopy for Nanomaterials Characterization*, Springer Berlin Heidelberg, (2013).
- 27 NAH Al-Aaraji, A Hashim & A Hadi, *Silicon* (2022).
- 28 J Tauc, *Optical properties of amorphous semiconductors*, In *Amorphous and liquid semiconductors*, Springer, Boston, MA(1974) 159.
- 29 R B Alam, M H Ahmad & M R Islam, *RSC Advances*, 12(23)(2022) 14686.
- 30 N S Alghunaim, *Results Phys*,9(2018), 1136.